
June 21-24
2025
SNMMI
Annual Meeting
New Orleans, Louisiana
ACCELERATING THE CURE

# Summary

1. **Graph-Based Radiomic Features** Enhance cancer diagnosis and treatment evaluation in **PET Imaging**
2. **Development of an organ-specific 18-FDG PET normative uptake atlas** and clinical application to the detection of organ inflammation
3. **Generative Artificial Intelligence**-Enabled Medical Image Generation for Improved Generalization of Deep Learning Models in Data-Constrained Environments
4. **Integrating Radiomic Features and Graph Neural Networks** for Single Time-Point **Dosimetry** in Lu-117 PSMA Therapy

# Graph-Based Radiomic Features in PET Imaging

**Title:** Graph-Based Radiomic Features Enhance cancer diagnosis and treatment evaluation in PET Imaging

**Runqi Meng**,
Shanghaitech University,
Center for Advanced Medical Computing and Analysis,
Department of Radiology,
Massachusetts General Hospital, Harvard Medical School

**Context:**
- Tumor heterogeneity measurements
- Radiomics in PET
- HN cancer, RFA treatment, NSCLC

**Current Challenge:**
- Lack of specificity for PET's unique functional characteristics
- Structural/Spatial heterogeneity

**Proposed Solution:** Novel set of graph theory-based radiomic features designed to capture both spatial and functional information in PET images

**Benefits:**
- Advancing/Enhancing PET image analysis.

**Glossary:**
**HN** = head and neck
**RFA** = radiofrequency ablation
**NSCLC** = non-small-cell lung cancer

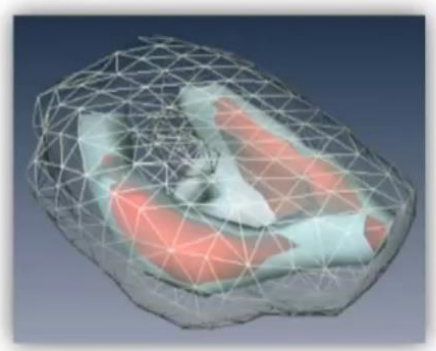

Graph-based Tumor
(Enables structural heterogeneity modeling)

# Graph-Based Radiomic Features in PET Imaging

## Data and Methods:

- **3 datasets of PET/CT images:**
  - HN cancer,
  - RFA treatment on lung cancer
  - NSCLC.
- Tumor ROIs manually contoured by radiologists.
- Model Artificial Neural Networks (ANN) with:
  - 7:3 ratio for training and testing sets
  - gradient search cross-validation for hyperparameter tuning,
  - 5-fold cross-validation to ensure robustness and minimize overfitting.
  - Evaluation with accuracy, specificity, sensitivity, and the AUC.

➔ Focus on **recurrence prediction tasks for HN and RFA**, and **survival prediction tasks for NSCLC**.

Table . Summary of Patient Distribution Across Datasets

| | Total Patients | Recurrent Cases | Non-Recurrent Cases |
|---|---|---|---|
| RFA Dataset | 49 | 12 | 37 |
| HN Dataset | 59 | 19 | 40 |
| | **Total Patients** | **Survived Cases** | **Deceased Cases** |
| NSCLC Dataset | 112 | 81 | 31 |

**Glossary:**
**HN** = head and neck
**RFA** = radiofrequency ablation
**NSCLC** = non-small-cell lung cancer

# Graph-Based Radiomic Features in PET Imaging

**Graph theory-based framework:**

- **To extract novel radiomic features by modeling tumor regions as graphs.**
- **Voxels** in the 3D matrix represented **nodes** and **edges** were defined by **intensity differences.**

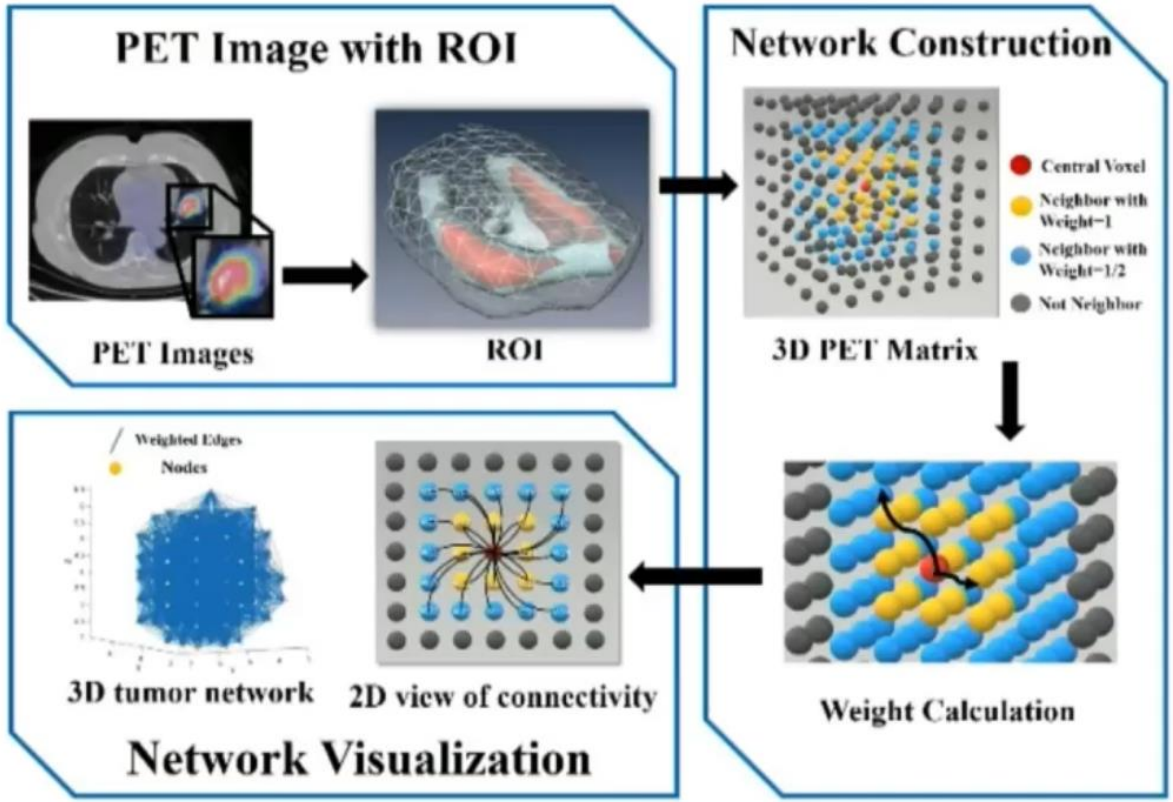


**Glossary:**
**HN** = head and neck
**RFA** = radiofrequency ablation
**NSCLC** = non-small-cell lung cancer

# Graph-Based Radiomic Features in PET Imaging

## Graph theory-based framework:

- **32 graph metrics** were computed to quantify **intratumoral heterogeneity and structural properties**.
- These graph-based features were **integrated with conventional texture-based radiomic features to enable a more comprehensive analysis of tumor characteristics**.

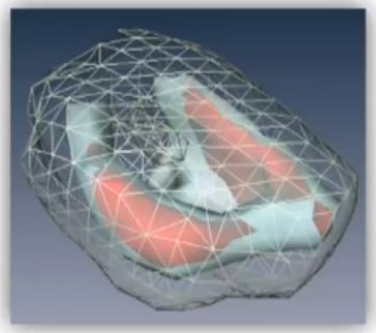

**Feature Extraction Based on Graph (n=32)**

- ✓ Spanning Tree Features (2 features)
- ✓ Spectral & Energy Features (7 features)
- ✓ Node Degree Features (7 features)
- ✓ Density & Clustering Features (5 features)
- ✓ Shape & Motif Features (7 features)
- ✓ PageRank Features (4 features)

**Glossary:**
**HN** = head and neck
**RFA** = radiofrequency ablation
**NSCLC** = non-small-cell lung cancer

# Graph-Based Radiomic Features in PET Imaging

**Results:** Patient-wise Comparison of Survival Prediction: PET ROI and Graph Features

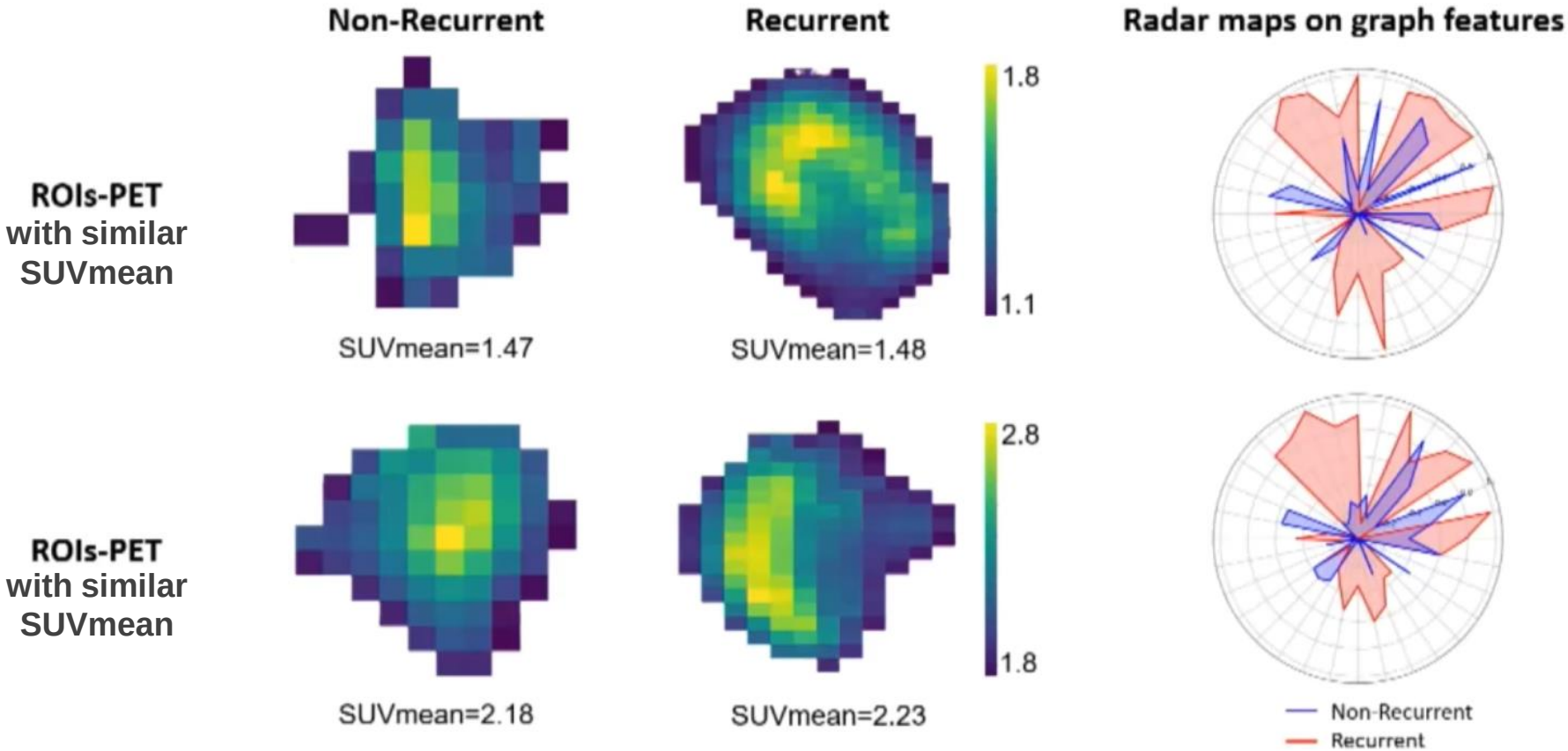

# Graph-Based Radiomic Features in PET Imaging

## Results:

The **combination of graph-based and texture-based radiomic features consistently outperformed texture-based features alone** across all three datasets.

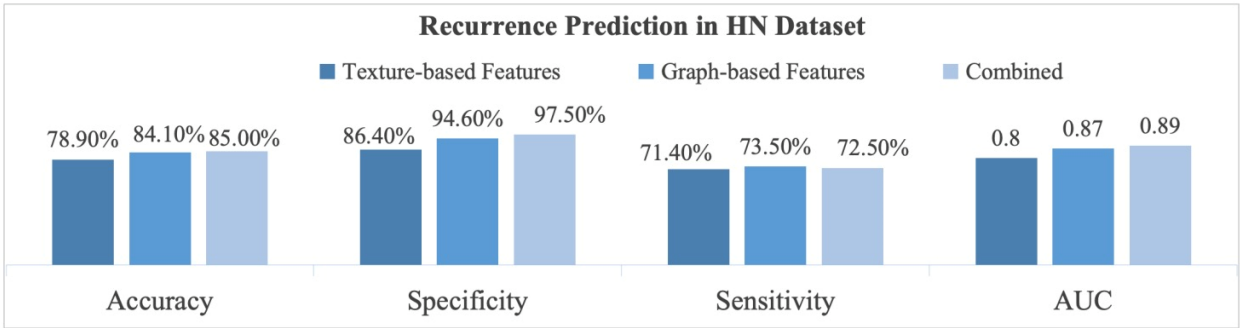


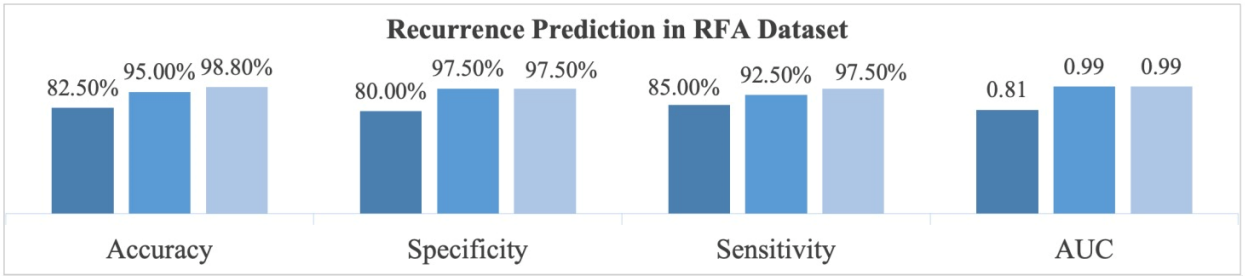


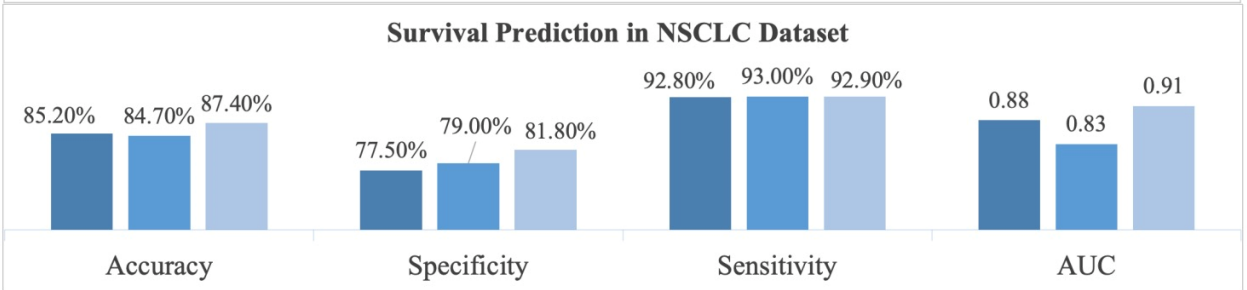


## Conclusions:

- **New representation of tumor heterogeneity.**
- Graph structure captures **complementary spatial information** to radiomics and **enhances predictive accuracy**.

**Glossary:**
**HN** = head and neck
**RFA** = radiofrequency ablation
**NSCLC** = non-small-cell lung cancer


June 21-24
2025
SNMMI
Annual Meeting
New Orleans, Louisiana
ACCELERATING THE CURE

# Organ-specific 18-FDG PET normative uptake atlas

**Title:** Development of an organ-specific 18-FDG PET normative uptake atlas and clinical application to the detection of organ inflammation

**Lucie Chambon,**
Department of Nuclear Medicine, Centre Antoine Lacassagne, Université Côte d'Azur (UCA)

**Context:**
- Non-small cell lung cancer (NSCLC)
- Treatments are known to induce various immune-related adverse events (irAEs)
- 18-FDG PET/CT is an effective tool to early detect the organ inflammation

**Current Challenge:**
- Time consuming
- Lack of reproducibility and quantification
- Definition of normality

**Proposed Solution:** Develop an organ-specific 18-FDG PET normative uptake atlas

**Benefits:**
- Reference for organ-specific 18-FDG PET normative uptake
- Automatic detection of organ inflammation

**Glossary:**
**irAEs =** immune-related adverse events
**NSCLC** = non-small cell lung cancer

# Organ-specific 18-FDG PET normative uptake atlas

**Data:**

1) **Atlas development**
   - Whole body 18-FDG PET/CT scans included after a **visual check for no-inflammation** by nuclear physicians (Olivier Humbert) from
     - 72 healthy subjects from **Centre Antoine Lacassagne**
     - 65 normal subjects from **autoPET**
   - 120 organs segmented using TotalSegmentator.

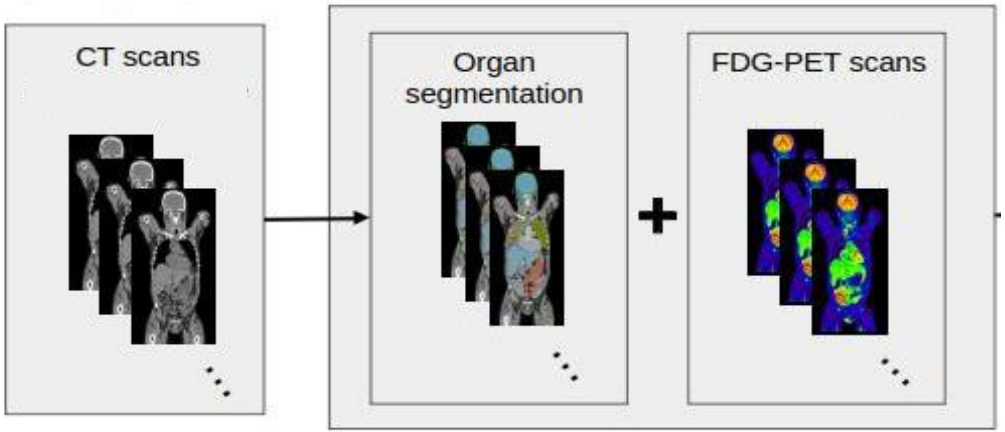


**Glossary:**
**irAEs =** immune-related adverse events
**NSCLC** = non-small cell lung cancer

# Organ-specific 18-FDG PET normative uptake atlas

**Data:**

**2) Atlas usage =** automatic detection of organ inflammation for NSCLC patients treated by immunotherapy

- Whole-body 18-FDG PET/CT scans from **95 NSCLC** patients treated by immunotherapy at Centre Antoine Lacassagne.
- **3 PET/CT exams**: at baseline, after 7 weeks, and 3 months of treatment.
- **7 organs** (colon, duodenum, esophagus, pancreas, small bowel, thyroid gland and stomach) segmented using TotalSegmentator.
- Immune-induced inflammation in these organs was visually assessed by nuclear medicine physicians (ground truth).

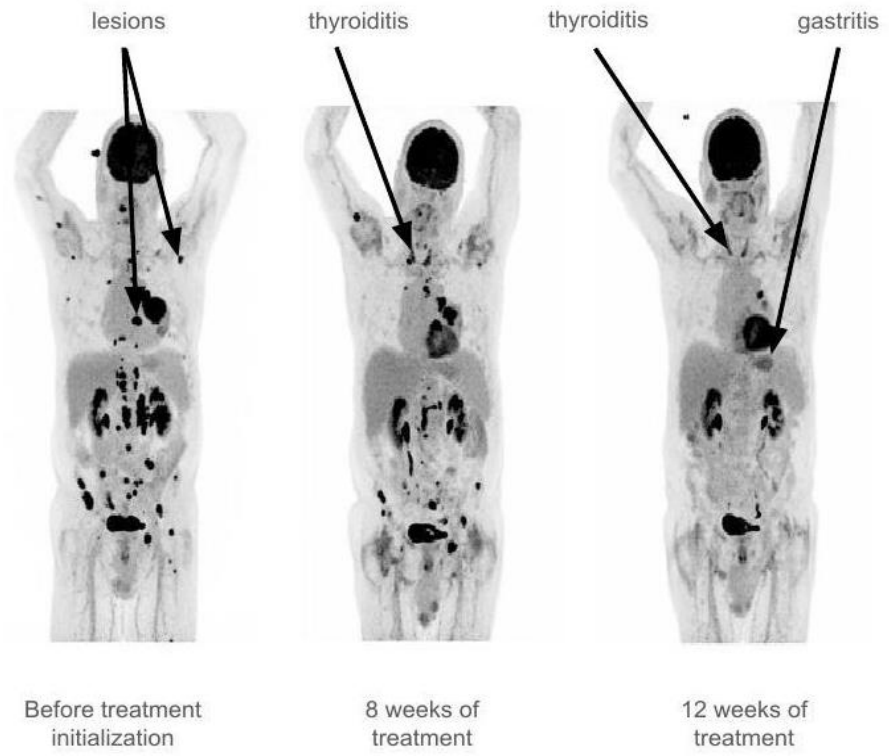


**Glossary:**
**irAEs =** immune-related adverse events
**NSCLC** = non-small cell lung cancer

# Organ-specific 18-FDG PET normative uptake atlas

**Methods:**

1) **Healthy atlas:**
   - Extraction of individual organ-specific **PET intensity distributions**
   - Organ-specific FDG uptake normative atlas modeled with **Wasserstein barycenters methods**

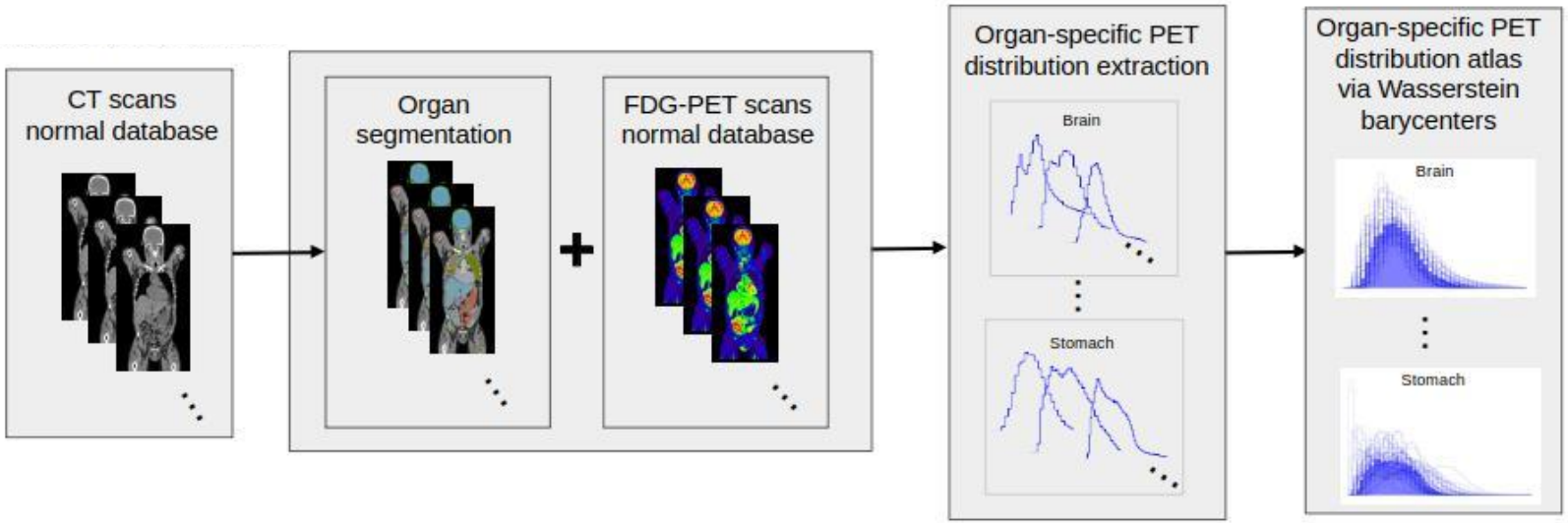


**Glossary:**
**irAEs =** immune-related adverse events
**NSCLC** = non-small cell lung cancer

# Organ-specific 18-FDG PET normative uptake atlas

## Methods:

**2) Atlas usage** = Automatic detection of organ inflammation for NSCLC patients treated by immunotherapy

- Individual organ-specific **PET intensity distributions** extracted through image segmentation.
- **Deviation** from the normal population reference assessed by computing a **Wasserstein-type distance**.
- Model to **select threshold per organ.**
- Evaluation using the area under the ROC curve (AUC).

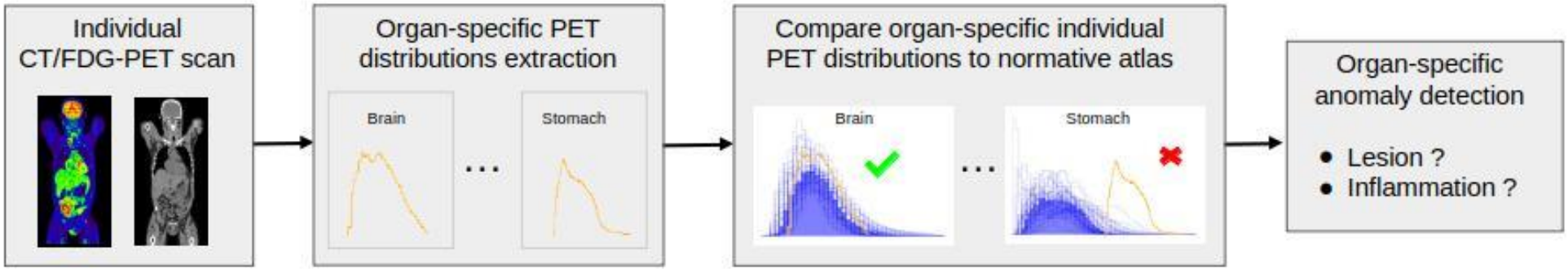


**Glossary:**
**irAEs =** immune-related adverse events
**NSCLC** = non-small cell lung cancer

# Organ-specific 18-FDG PET normative uptake atlas

## Wasserstein distance:

- The **Wasserstein distance**, also known as the **optimal transport distance**, is a measure of similarity between two probability distributions.

Given two 1D probability mass functions, $u$ and $v$, the first Wasserstein distance between the distributions is:

$$W_1(u,v) = \inf_{\pi \in \Gamma(u,v)} \int_{\mathbb{R}\times\mathbb{R}} |x-y| \mathrm{d}\pi(x,y)$$

where $\Gamma(u,v)$ is the set of (probability) distributions on $\mathbb{R} \times \mathbb{R}$ whose marginals are $u$ and $v$ on the first and second factors respectively. For a given value $x$, $u(x)$ gives the probability of $u$ at position $x$, and the same for $v(x)$.

If $U$ and $V$ are the respective CDFs of $u$ and $v$, this distance also equals to:

$$W_1(u,v) = \int_{-\infty}^{+\infty} |U-V|$$

# Organ-specific 18-FDG PET normative uptake atlas

## Wasserstein barycenter:

- An '**average' of several probability distributions**, but according to the geometry of the Wasserstein distance.
- Merging several distributions while respecting their spatial structures.

Given $N$ probability distributions $\mu_1, \mu_2, \ldots, \mu_N$ on $\mathbb{R}$, with weights $\lambda_1, \ldots, \lambda_N$ (such that $\sum_i \lambda_i = 1$), the **Wasserstein-1 barycenter** $\nu^*$ minimizes:

$$\nu^* = \arg\min_{\nu} \sum_{i=1}^{N} \lambda_i \, W_1(\nu, \mu_i)$$

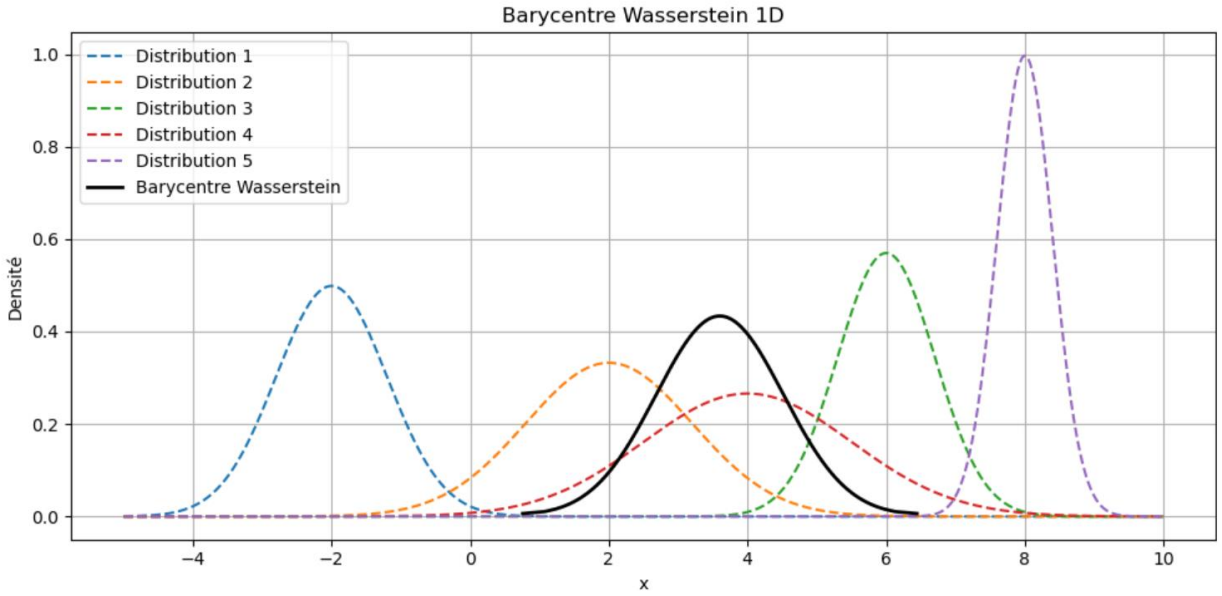

# Organ-specific 18-FDG PET normative uptake atlas

**Results:** Thyroid gland

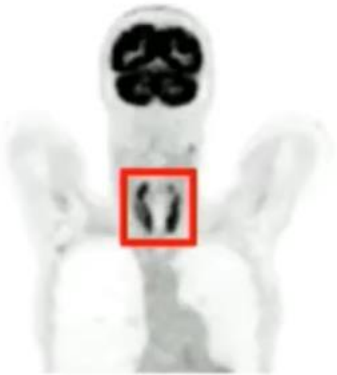

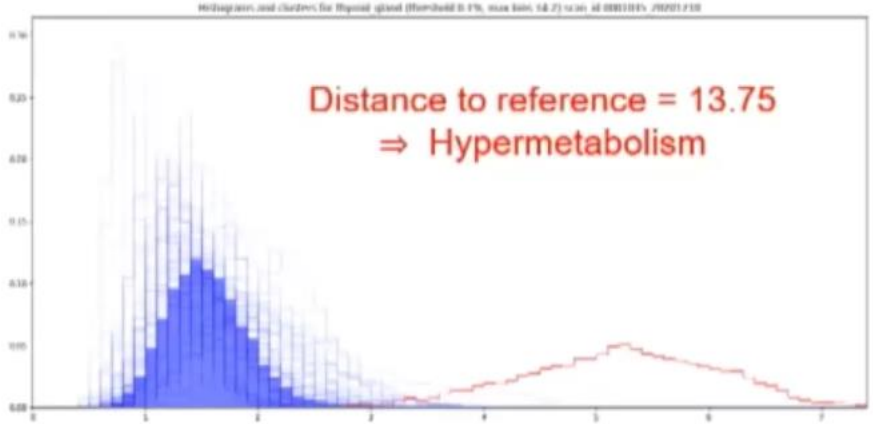


# Organ-specific 18-FDG PET normative uptake atlas

**Results:** Stomach

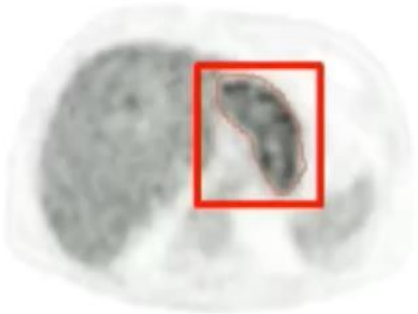

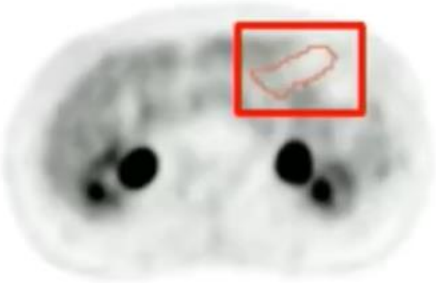

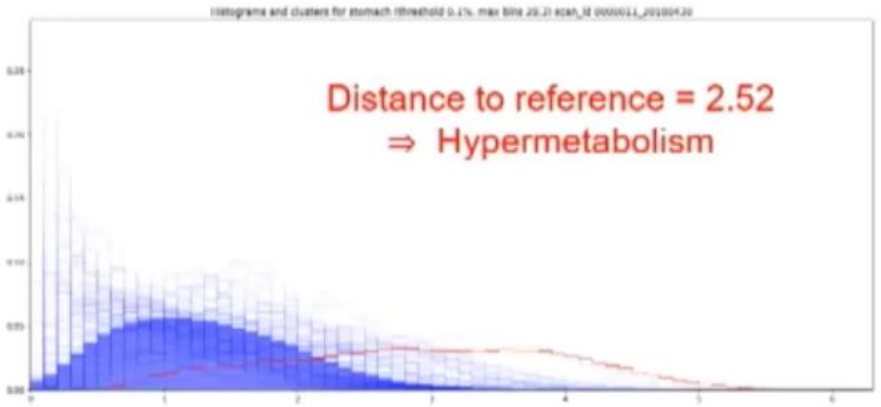


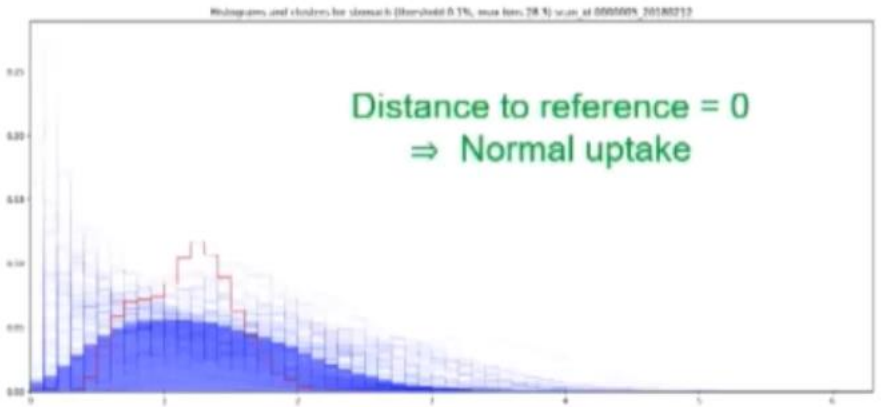

# Organ-specific 18-FDG PET normative uptake atlas

## Results and Conclusions:

- The AUC scores for immune-induced inflammation detection in the 7 organs were > 70%.

➔ Method's good performance in detecting inflammation in different types of organs + validation of normative atlas

| organ | threshold | sensitivity | specificity | ROC AUC | accuracy | # infl | # no infl |
|---|---|---|---|---|---|---|---|
| colon | 0.507 | 0.783 | 0.688 | 0.736 | 0.697 | 23 | 231 |
| duodenum | 0.23 | 0.75 | 0.768 | 0.749 | 0.768 | 8 | 246 |
| esophagus | 0.155 | 0.75 | 0.736 | 0.739 | 0.736 | 8 | 246 |
| pancreas | 0.004 | 1 | 0.972 | 0.986 | 0.972 | 1 | 253 |
| small bowel | 0.542 | 0.667 | 0.649 | 0.654 | 0.65 | 9 | 245 |
| stomach | 0.2 | 0.8 | 0.738 | 0.857 | 0.748 | 40 | 214 |
| thyroid gland | 0.095 | 0.913 | 0.943 | 0.979 | 0.94 | 23 | 228 |

**Glossary:**
**irAEs =** immune-related adverse events
**NSCLC** = non-small cell lung cancer


June 21-24
2025
SNMMI
Annual Meeting
New Orleans, Louisiana
ACCELERATING THE CURE

# Generative Artificial Intelligence

**Title:** Generative Artificial Intelligence-Enabled Medical Image Generation for Improved Generalization of Deep Learning Models in Data-Constrained Environments

**David Haberl,**
Division of Nuclear Medicine, Department of Biomedical Imaging and Image-Guided Therapy, Medical University of Vienna, Vienna, Austria

**Context:**

- 99mTc bone scintigraphy = nuclear medicine imaging technique used to help diagnose and assess different bone diseases because allowing visualisation of bone metabolism or bone remodelling, which most other imaging techniques (such as CT) cannot.

**Current Challenge:**

- Scarcity of large labelled datasets (critical for rare disease)
- Multi-institutional data sharing

**Proposed Solution:** Create annotated synthetic medical images using a generative artificial intelligence approach

**Benefits:**

- Enriching small-scale datasets with synthetic data
- Improve model training
- Enhance the generalization of models in real-world clinical practice

# Generative Artificial Intelligence

## Data:

### Generative task:

- Training data = **99mTc-bone scintigraphy scans** (2D projection) from 9,170 patients in Site A representing two clinical conditions: **abnormal uptake** indicative of bone metastases and cardiac uptake indicative of cardiac amyloidosis.

### Prediction task:

- Training data = independent small single-center dataset (Site B) + synthetic scans from Site A
- Testing data = 7,472 scans from 6,448 patients across four external sites (Site C-F) in a cross-tracer and cross-scanner setting.

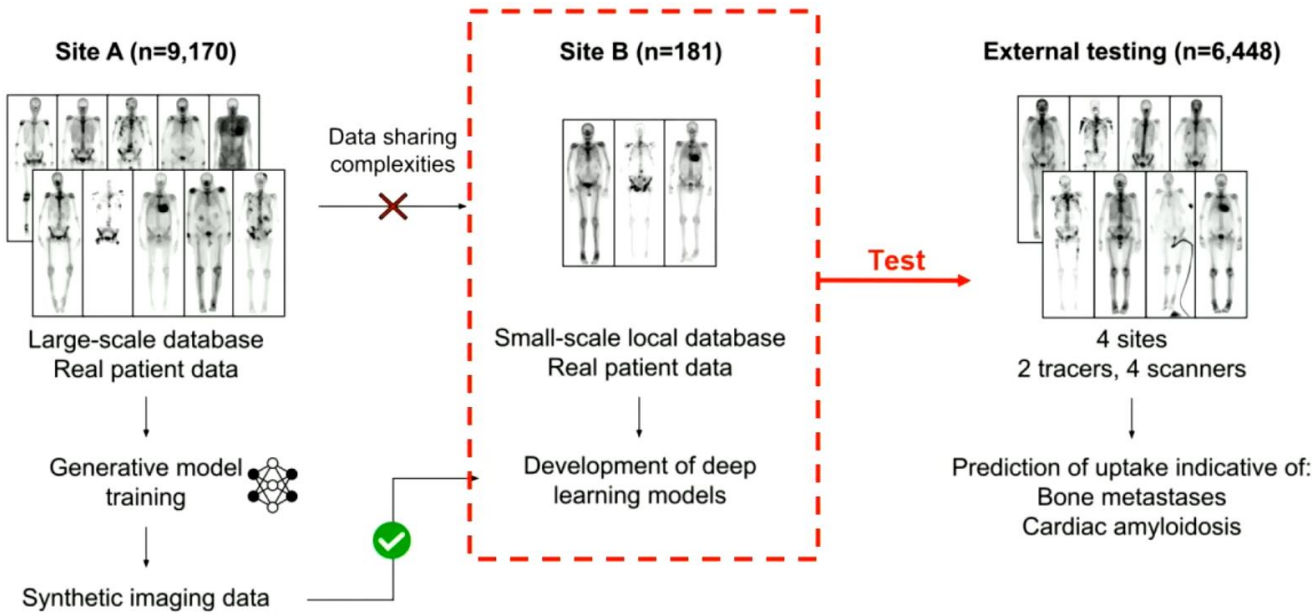

# Generative Artificial Intelligence

## Methods:

### Generative task:

- Train a generative model (StyleGAN2)

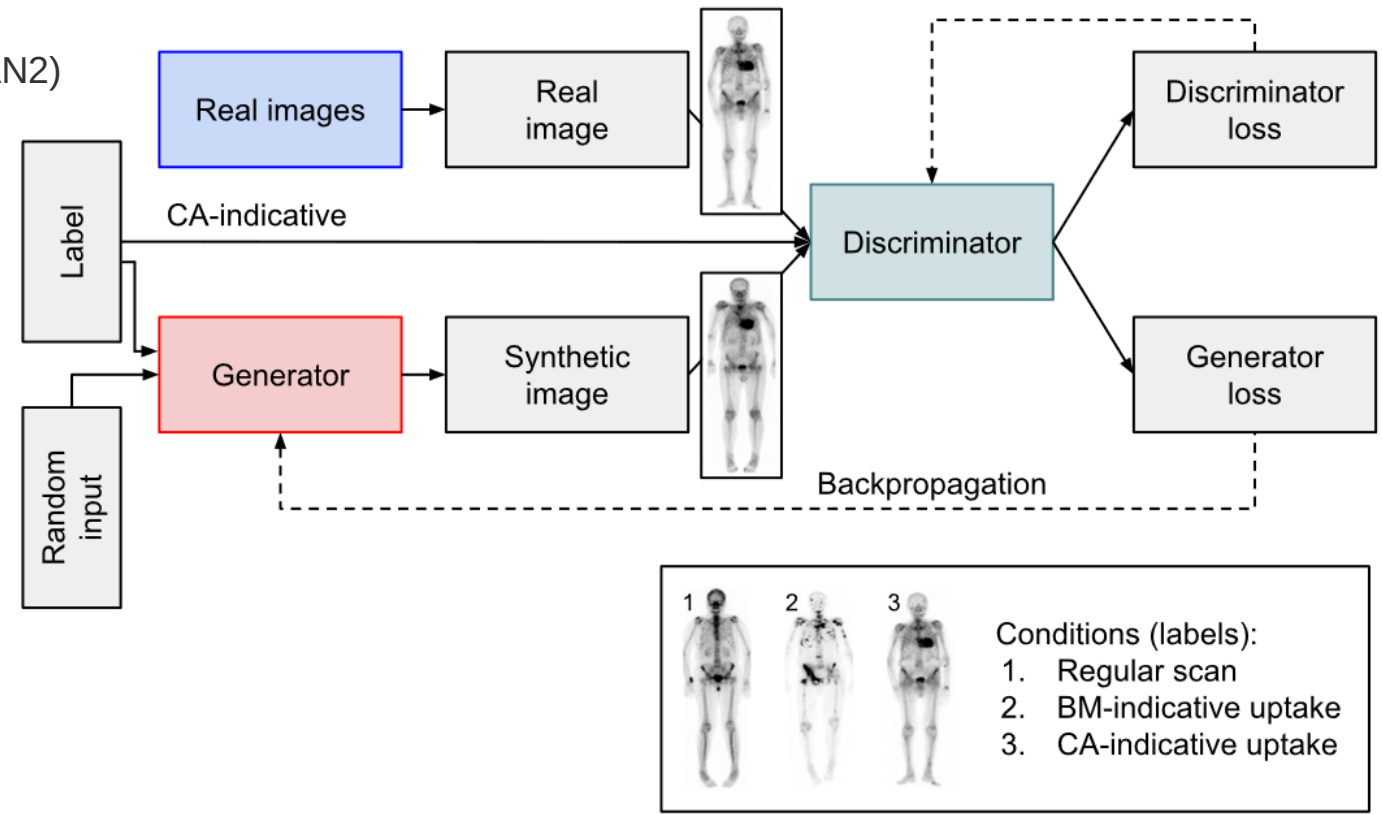

# Generative Artificial Intelligence

## Methods:

**Generative task:**

- Train a generative model (StyleGAN2)
- 4 nuclear medicine physicians evaluated the quality and clinical validity of the generated synthetic images using a score specifying whether a given image was real or synthetic.

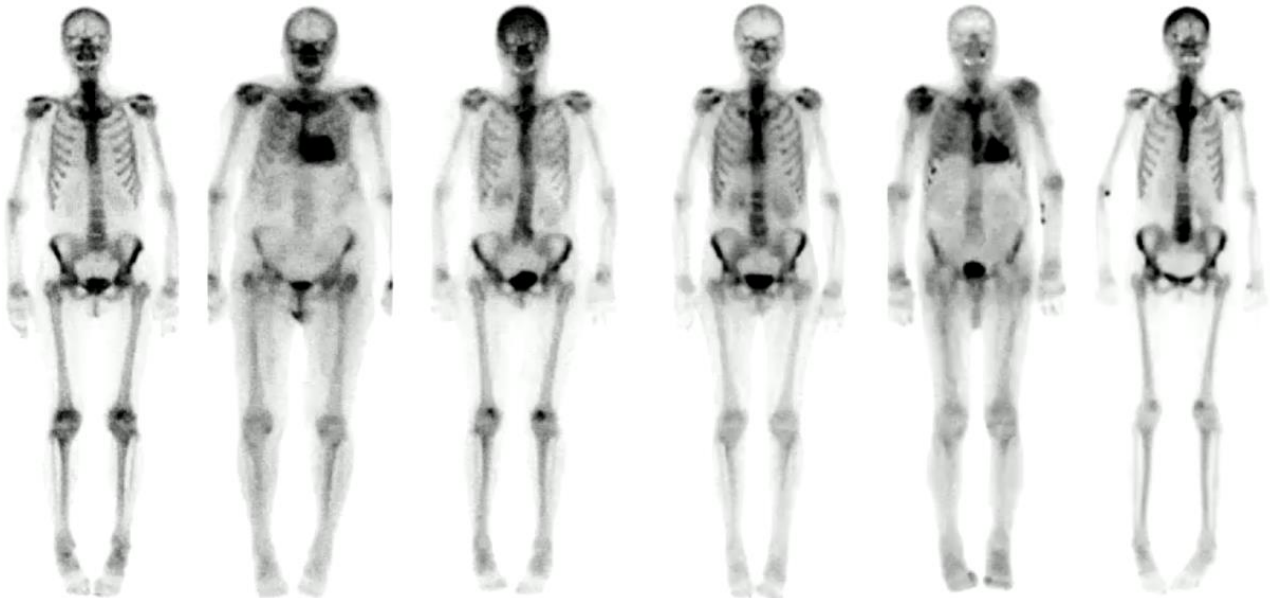

Which are real and which are synthetic?

# Generative Artificial Intelligence

## Methods:

### Generative task:

- Train a generative model (StyleGAN2)
- 4 nuclear medicine physicians evaluated the quality and clinical validity of the generated synthetic images using a score specifying whether a given image was real or synthetic.

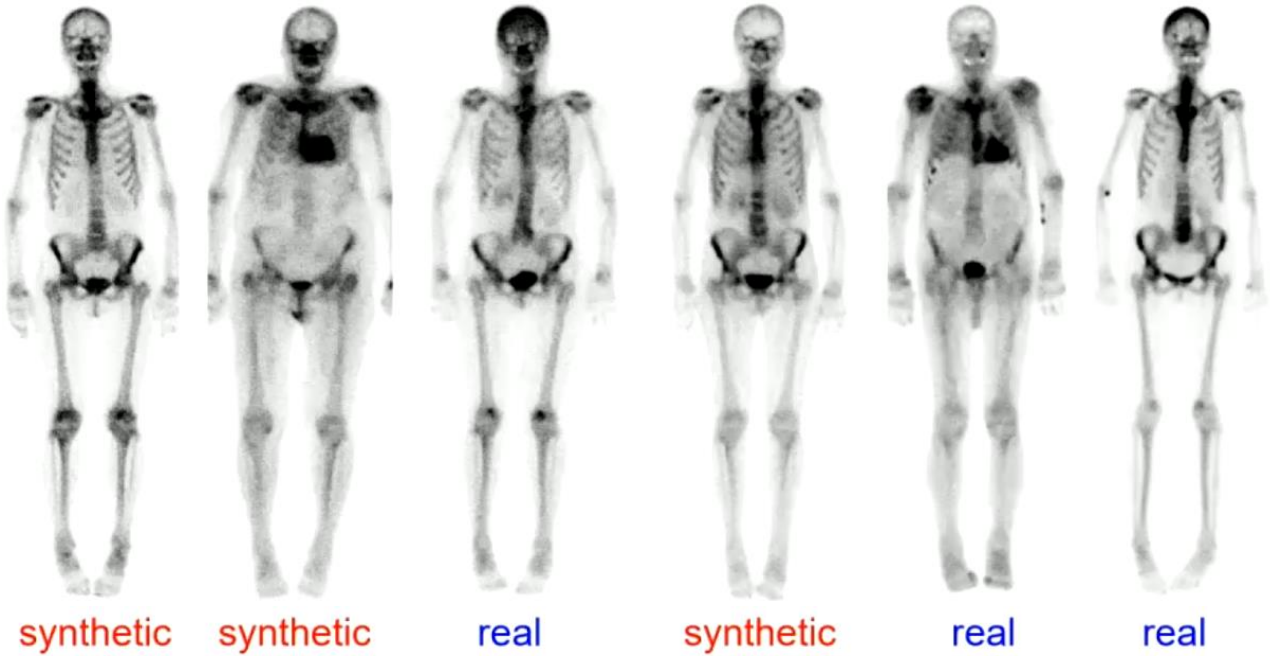

# Generative Artificial Intelligence

## Methods:

### Generative task:

- Train a generative model (StyleGAN2)
- 4 nuclear medicine physicians evaluated the quality and clinical validity of the generated synthetic images using a score specifying whether a given image was real or synthetic.

### Prediction task:

- Training a deep learning model to detect abnormal uptake using real data and real + synthetic data.
- Convolutional neural network based on the DenseNet121 architecture
- Models were pre-trained on the ImageNet database

## Results and Conclusions: Generative task

- The four readers **could not differentiate synthetic scans from real scans** (average accuracy: 0.48 [95% CI: 0.45-0.51] for BoneMetastase-indicative uptake and 0.49 [95% CI: 0.46-0.52] for CardiacAmyloidosis-indicative uptake).
- They **disagreed in 60% of cases**, having a high inter-observer variability.

➔ Generative AI facilitates the creation of synthetic bone scintigraphy images that accurately **mimic realistic clinical feature**.

➔ These **synthetic scans were indistinguishable from real patient scans**, demonstrating their high quality and clinical validity.

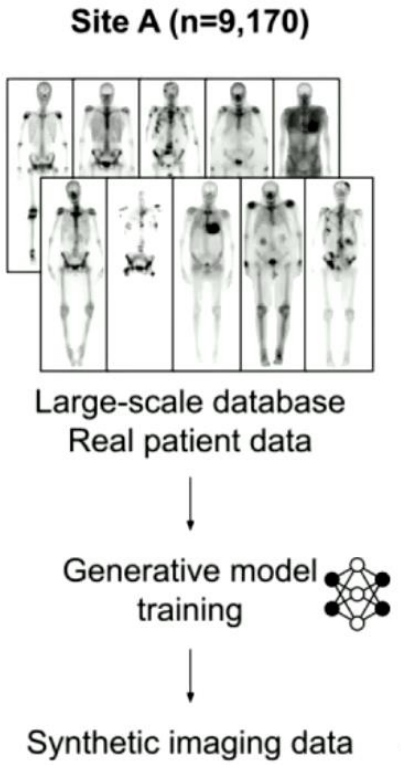

## **Results:** **Prediction task** for Bone Metastasis

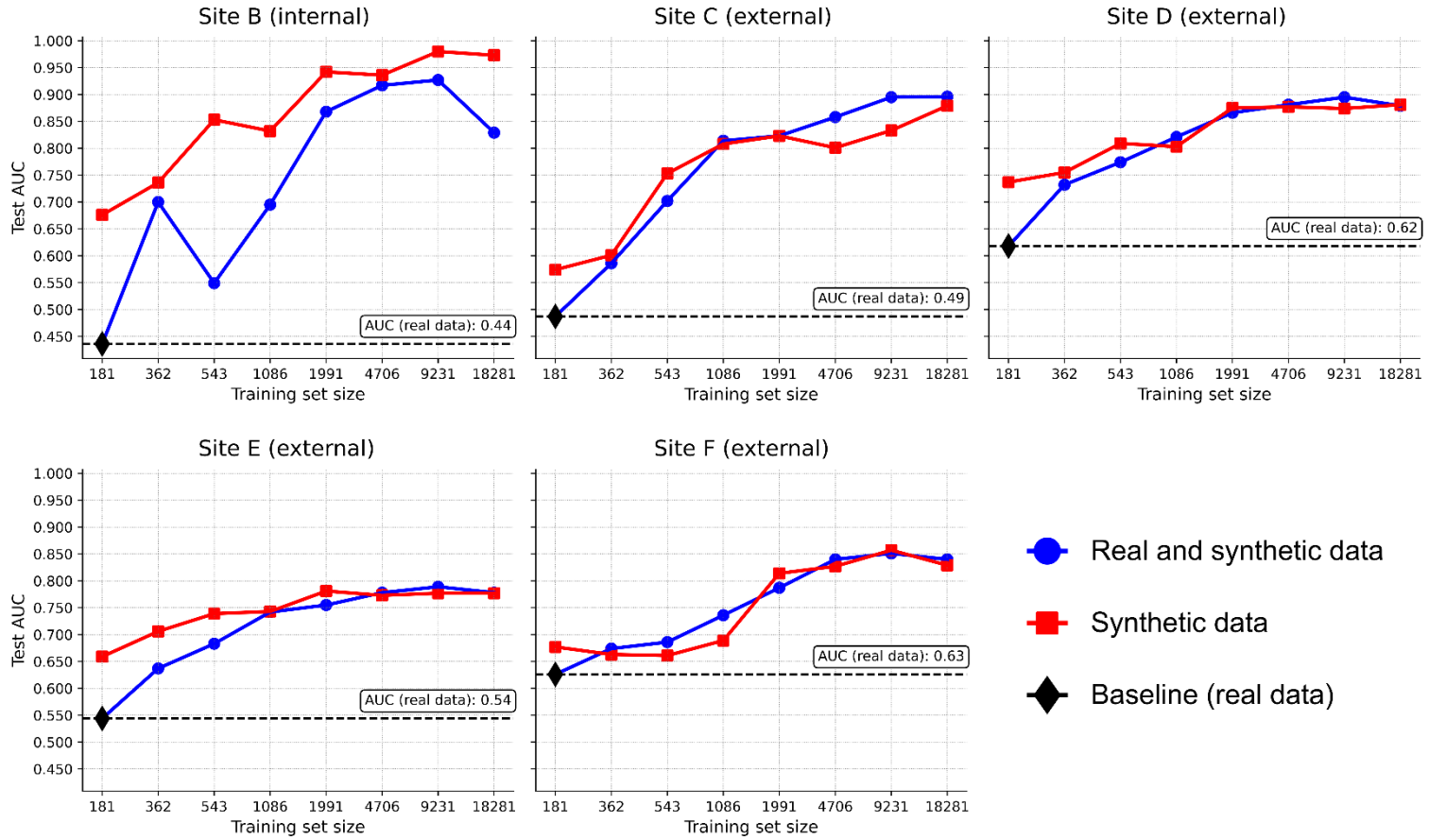

**Results:** **Prediction task** for Cardiac Amyloidosis

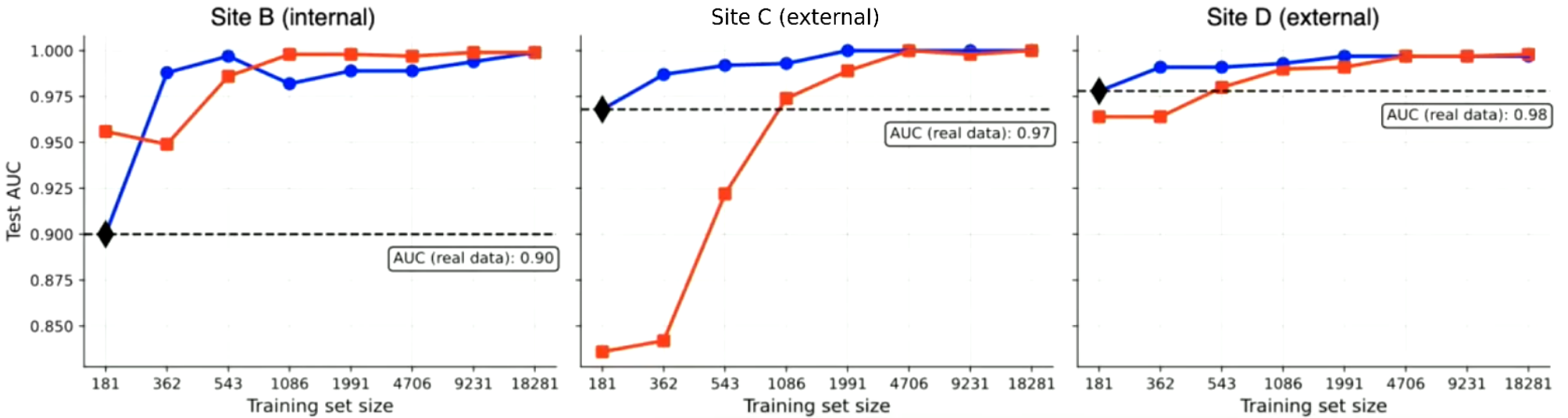

**Results:** **Prognostic value of the prediction model**

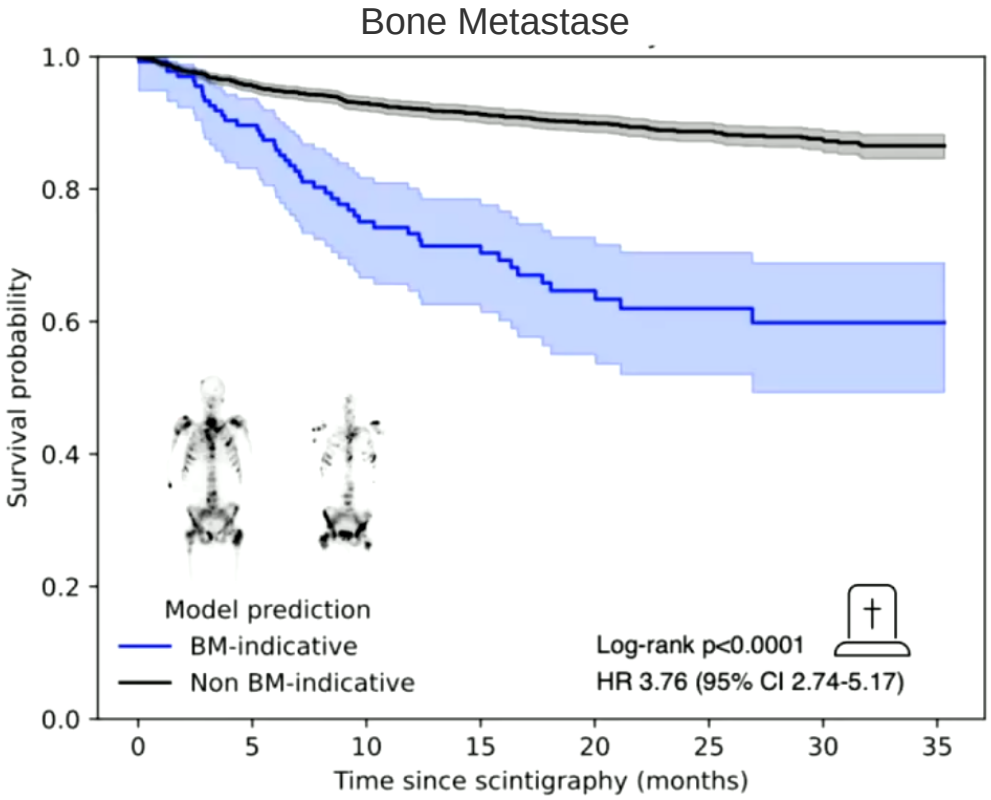


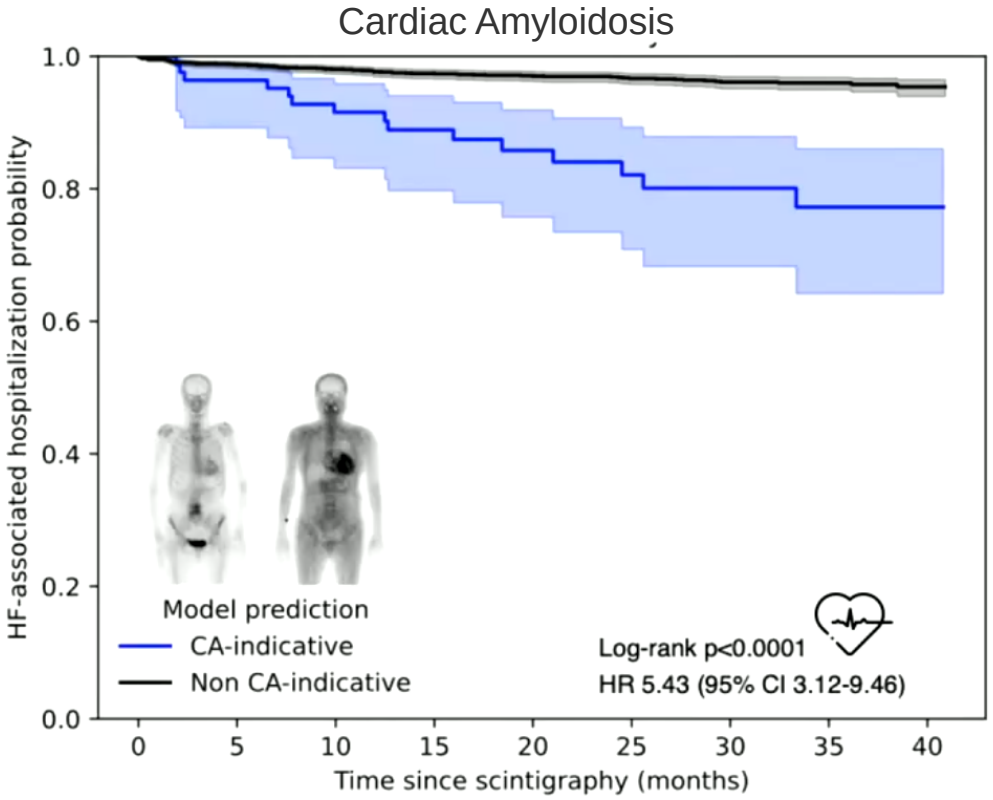

## Results and Conclusions: Prediction task

Incorporating synthetic data into the training of a deep learning model **increased the performance** by an average (± SD) of **33%** (±10) AUC for detecting abnormal uptake suggestive of **bone metastases** and by **5%** (±4) AUC for identifying uptake indicative of **cardiac amyloidosis**.

➔ Synthetic data can be used to **augment small single-center databases** to **improve model generalization across internal and external patient cohorts**.

➔ These results highlight the potential of synthetic data to **address data sharing challenges** and improve fairness in medical classifiers.

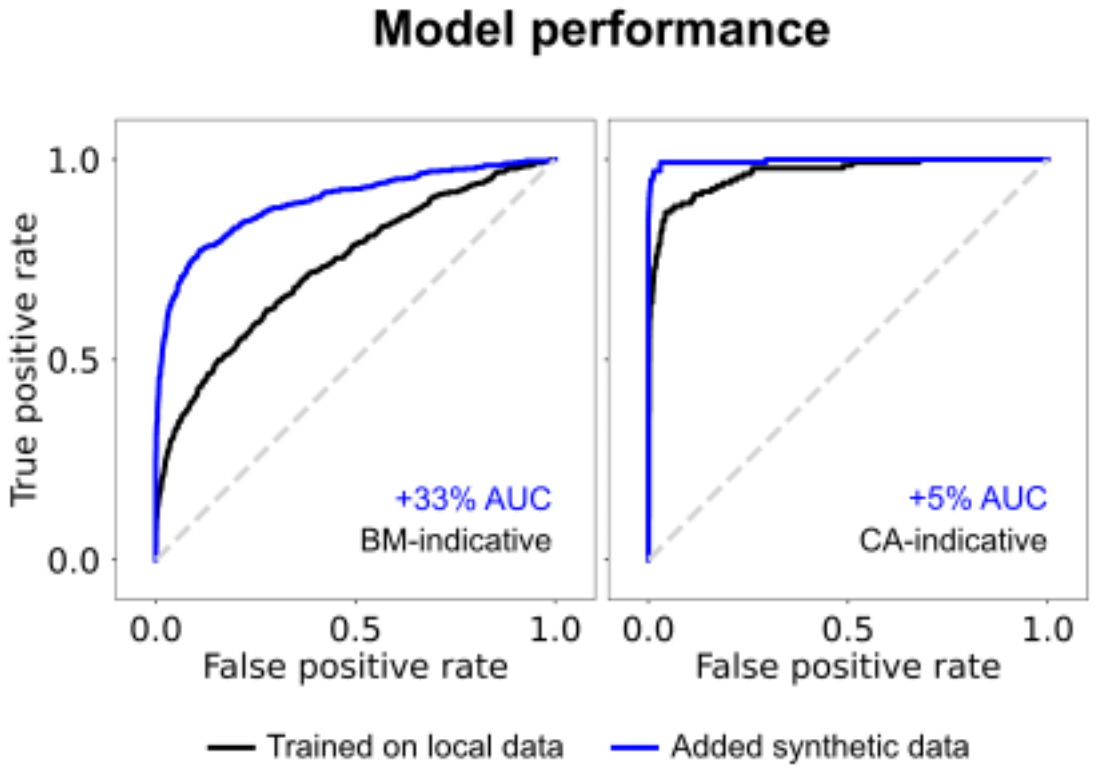


June 21-24
2025
SNMMI
Annual Meeting
New Orleans, Louisiana
ACCELERATING THE CURE

# Radiomic Features and Graph Neural Networks for Dosimetry

**Vibha Balaji,**
Department of Biomedical Engineering, University of Massachusetts Amherst

**Title:** Integrating Radiomic Features and Graph Neural Networks for Single Time-Point Dosimetry in Lu-117 PSMA Therapy

**Context:**
- Lu-177 PSMA: A targeted radiopharmaceutical that delivers radiation specifically to prostate cancer cells expressing PSMA.
- Imaging modality: SPECT/CT.

**Current Challenge:**
- Standard dosimetry requires multiple SPECT/CT scans to calculate TIA.
- STP methods (e.g., STP-M, STP-H) are limited by their inability to account for patient variability, cross-organ interactions, and their dependence on empirical models developed for specific radiotracers.

**Proposed Solution:** A novel Graph Neural Network (GNN) model that uses radiomic features from a single SPECT/CT scan to predict TIA in 8 organs-at-risk.

**Benefits:**
- More accurate and personalized dosimetry.
- Minimizing radiation exposure to OARs.

**Glossary:**
**OARs =** organs at risks
**MTP =** multiple time-point
**TIA =** time-integrated activity
**STP =** single time-point
**STP-M =** Madsen single time-point
**STP-H** = Hänscheid single time-point
**TACs** = time activity curves

# Radiomic Features and Graph Neural Networks for Dosimetry

**Data:**

- **34 patients** undergoing Lu-177 PSMA therapy, encompassing 84 dose cycles with 2–3 imaging time points acquired between 24- and 216-hours post-injection.
- **OARs = spleen, right kidney, left kidney, gallbladder, liver, stomach, pancreas, and prostate** segmented TotalSegmentator.
- **37 radiomic features** (included first-order statistics, shape-based features, and texture features) were extracted using PyRadiomics and normalized using z-score.
- **Spatial proximity** between each pair of OARs was used as the edges of OAR-graph for each patient

➔ **Input of GNN model**

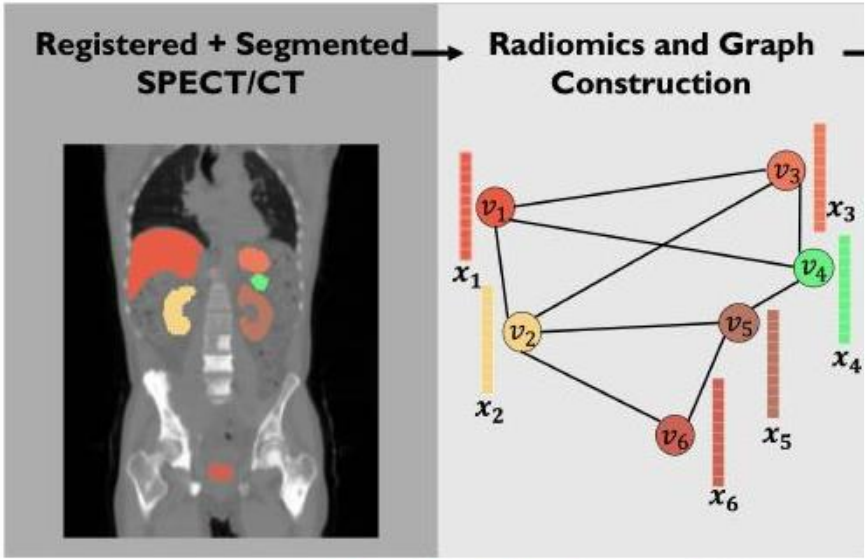


**Glossary:**
**OARs =** organs at risks
**MTP =** multiple time-point
**TIA =** time-integrated activity
**STP =** single time-point
**STP-M =** Madsen single time-point
**STP-H** = Hänscheid single time-point
**TACs** = time activity curves

# Radiomic Features and Graph Neural Networks for Dosimetry

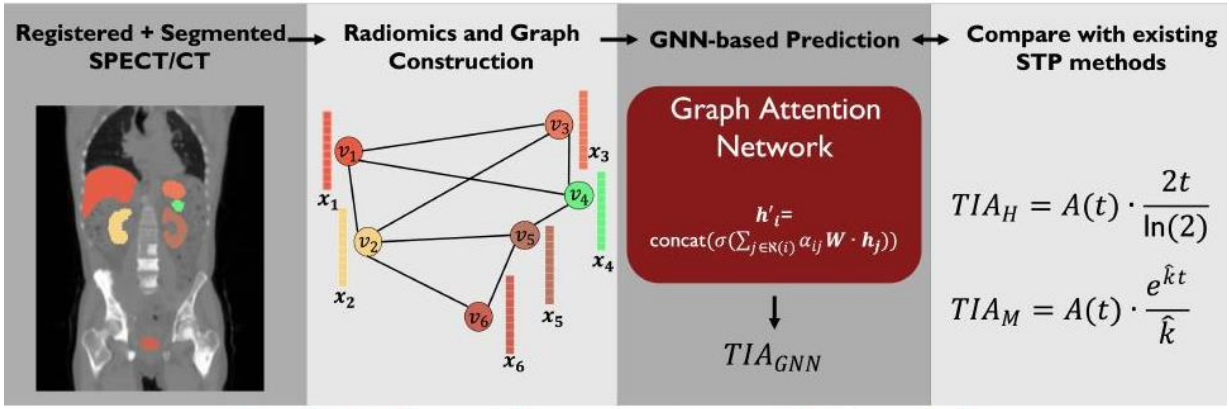


Fig. 2. Workflow of data processing and STP methods

- The train set encompassed 58 (70%) and the test set had 26 (30%) out of the 84 dose cycles across all subjects.
- The high-dimensional node inputs were passed through an encoder for feature reduction from 37 to 12.
- A graph attention network (GAT) was chosen as the GNN and implemented to predict OAR-specific TIA using z-score normalized radiomic features and inter-organ connectivity.
- The GAT model used 3 layers, 128 hidden channels, learning rate 5e-4, 500 epochs to predict the TIA (STP-GNN), compared with MTP TIA as ground truth using the L2 loss function.

## Methods:

- **MTP dosimetry** was performed by fitting the TAC (= **ground truth**).
- **GNN-based STP method**
- The **performance** of the GNN-based STP method is compared with STP-H, STP-M, and MTP using metrics such as RMSE, NRMSE and MAE.

**Glossary:**
**OARs =** organs at risks
**MTP =** multiple time-point
**TIA =** time-integrated activity
**STP =** single time-point
**STP-M =** Madsen single time-point
**STP-H** = Hänscheid single time-point
**TACs** = time activity curves
**NRMSE** = normalized root-mean-squared error
**MAE** = mean absolute error

# Radiomic Features and Graph Neural Networks for Dosimetry

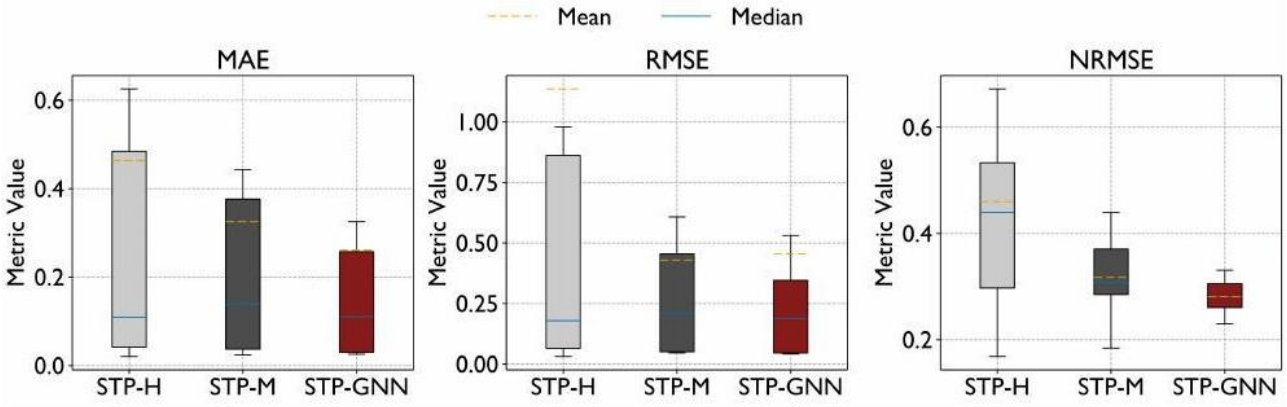


| OAR | STP-H | STP-M | STP-GNN |
|---|---|---|---|
| Spleen | 0.306 | 0.367 | 0.331 |
| Right Kidney | 0.487 | 0.302 | 0.264 |
| Left Kidney | 0.895 | 0.439 | 0.309 |
| Gall Bladder | 0.168 | 0.254 | 0.251 |
| Liver | 0.672 | 0.184 | 0.230 |
| Stomach | 0.272 | 0.314 | 0.269 |
| Pancreas | 0.464 | 0.382 | 0.305 |
| Prostate | 0.416 | 0.296 | 0.292 |



Fig. 3. (Top) Whisker plots of MAE, RMSE, and NRMSE across subjects (Bottom) OAR-wise NRMSE values for STP-H, STP-M, and STP-GNN

**Results:**

The **GNN-based STP** method demonstrated the **lowest NRMSE and MAE** (0.02455, 0.2597) across all dose cycles, **outperforming STP-M** (0.0296, 0.3135) **and STP-H** (0.0457, 0.4841).

**Conclusion:** improving TIA estimation, outperforming existing STP methods and offering patient-specific, radiotracer-agnostic solution for dosimetry.

**Glossary:**

**OARs =** organs at risks
**MTP =** multiple time-point
**TIA =** time-integrated activity
**STP =** single time-point
**STP-M =** Madsen single time-point
**STP-H** = Hänscheid single time-point
**TACs** = time activity curves
**NRMSE** = normalized root-mean-squared error
**MAE** = mean absolute error


June 21-24
2025
SNMMI
Annual Meeting
New Orleans, Louisiana
ACCELERATING THE CURE

# Annexes

# Development of an organ-specific 18-FDG PET normative uptake atlas and clinical application to the detection of organ inflammation

Lucie Chambon[1], Francesco Cremonesi[1], Huyen Trang Nguyen[1], Olivier Humbert[2,3], Marco Lorenzi[1]
[1] Inria Center at Université Côte d'Azur, Epione Research Group, France
[2] Department of Nuclear Medicine, Centre Antoine Lacassagne, Université Côte d'Azur (UCA), 33 Avenue de Valombrose, 06189 Nice, France
[3] Université Côte d'Azur, CNRS, Inserm, iBV, Nice, France

## 1. INTRODUCTION

### A) CONTEXT

18-FDG PET images are widely used for detecting tumors or inflammation through **visual checks and semi-quantitative metrics based on SUV.** However, these methods are **time consuming and lack of robustness and reproducibility**. Therefore, there is a need for tools that can **automatically quantify abnormal metabolic uptake**.

For this purpose, and **given the heterogeneity of the data**, it is essential first to **define what is 'normality'**.

### B) OBJECTIVES

Develop an **organ-specific 18-FDG PET normative uptake atlas** from a representative set of images of healthy patients and validate this atlas for the **automatic detection and quantification of organ inflammation**

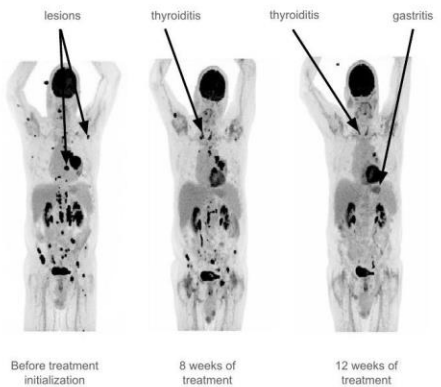


## 2. METHODS

### A) DEVELOP AN ORGAN-SPECIFIC 18-FDG PET NORMATIVE UPTAKE DISTRIBUTION ATLAS

Whole-body 18-FDG PET/CT scans from **72 healthy patients of Centre Antoine Lacassagne and 65 normal patients from autoPET** [1] database were included after visual check for no-inflammation by nuclear physicians. From CT scans, **organ were segmented** with TotalSegmentator [2], and the corresponding individual organ-specific **PET intensities distributions** were extracted. The final organ-specific FDG uptake **normative atlas** was computed with Wasserstein barycenter [3]

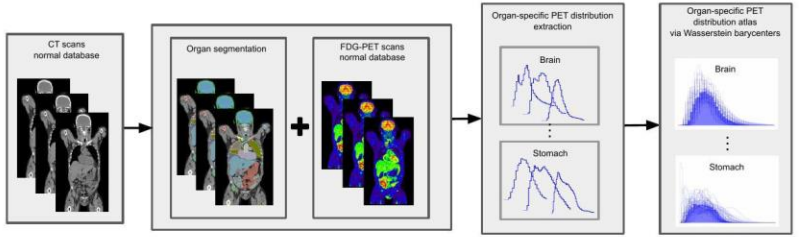


### B) ATLAS USAGE FOR AUTOMATIC QUANTIFICATION OF ORGAN INFLAMMATION

Individual organ-specific PET intensities distributions are extracted through image segmentation, and their **deviation from normal population reference** is assessed with Wasserstein distance.

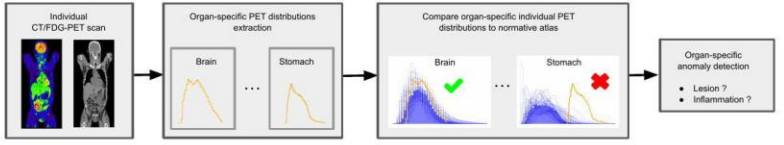


[1] Gatidis, Sergios, et al. "A whole-body FDG-PET/CT dataset with manually annotated tumor lesions." Scientific Data 9.1 (2022): 601.
[2] Wasserthal, Jakob, et al. "TotalSegmentator: robust segmentation of 104 anatomic structures in CT images." *Radiology: Artificial Intelligence* 5.5 (2023): e230024.
[3] Agueh, Martial, et al. "Barycenters in the Wasserstein space." *SIAM Journal on Mathematical Analysis* 43.2 (2011): 904-924.

## 3. RESULTS

Whole-body 18-FDG PET/CT scans from **95 non-small cell lung cancer (NSCLC) patients treated by immunotherapy of Centre Antoine Lacassagne** were included. Among this cohort, the detection of immune-induced inflammation in 7 organs was visually assessed by nuclear medicine physicians.

The ability of the method to automatically detect organ inflammation was evaluated with **area under the ROC curve (AUC),** and the metric threshold was optimized to **maximize sensitivity and specificity**

| organ | threshold | sensitivity | specificity | ROC AUC | accuracy | # infl | # no infl |
|---|---|---|---|---|---|---|---|
| colon | 0.507 | 0.783 | 0.688 | 0.736 | 0.697 | 23 | 231 |
| duodenum | 0.23 | 0.75 | 0.768 | 0.749 | 0.768 | 8 | 246 |
| esophagus | 0.155 | 0.75 | 0.736 | 0.739 | 0.736 | 8 | 246 |
| pancreas | 0.004 | 1 | 0.972 | 0.986 | 0.972 | 1 | 253 |
| small bowel | 0.542 | 0.667 | 0.649 | 0.654 | 0.65 | 9 | 245 |
| stomach | 0.2 | 0.8 | 0.738 | 0.857 | 0.748 | 40 | 214 |
| thyroid gland | 0.095 | 0.913 | 0.943 | 0.979 | 0.94 | 23 | 228 |

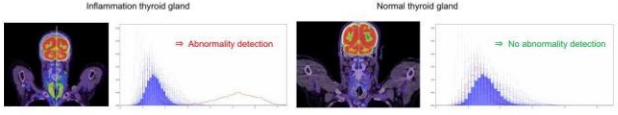


## 4. CONCLUSION

The method shows **good performance in detecting inflammation** in different types of organs, validating the use of the normative atlas.

Further developments include:
- **Increasing the hospital diversity of the normal database** for greater robustness
- Incorporating an external database for **external validation**
- Using this metric to predict survival outcome

Home > European Journal of Nuclear Medicine and Molecular Imaging > Article

# Generative artificial intelligence enables the generation of bone scintigraphy images and improves generalization of deep learning models in data-constrained environments

Original Article | Open access | Published: 29 January 2025

Volume 52, pages 2355–2368, (2025) Cite this article

Download PDF

You have full access to this open access article

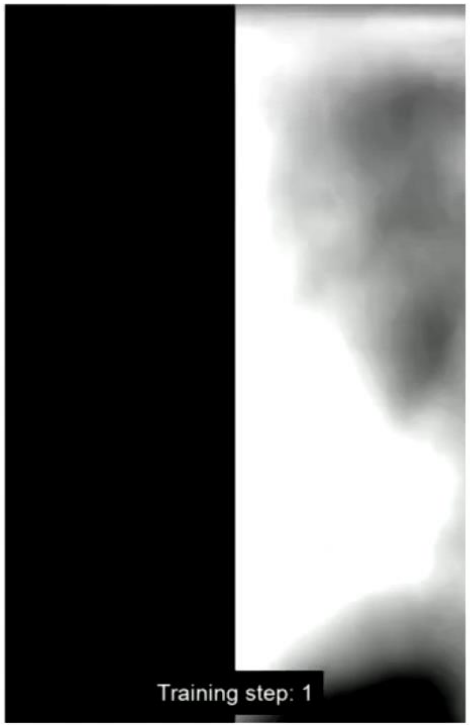


GenAI

# Integrating Radiomic Features and Graph Neural Networks for Single Time-Point Dosimetry in Lu-177 PSMA Therapy

Vibha Balaji[1], Bowen Lei[1], Fan Yang[1], Quanzheng Li[2], Michael King[3], Joyita Dutta[1]

[1]Department of Biomedical Engineering, University of Massachusetts Amherst, Amherst, MA, USA
[2]Center for Advanced Medical Computing and Analysis, Massachusetts General Hospital, Boston, MA, USA
[3]Department of Radiology, UMass Chan Medical School, Worcester, MA, USA

2025 SNMMI Poster Award Candidate
SNMMI Annual Meeting
Abstract #242004

## Introduction

### Background

- Radiopharmaceutical therapy (RPT) utilizes targeted radionuclides to treat cancer, with Lu-177-prostate-specific-membrane-antigen (PSMA) showing promise for metastatic castration-resistant prostate cancer.
- Quantitative dosimetry in RPT is used to gauge the amount of radiation dose absorbed by both tumor cells and organs-at-risk (OARs). Multiple time-point (MTP) SPECT imaging is employed for accurate dose estimation.
- Time-integrated activity (TIA) is a precursor to estimating the radiation dose and is calculated by fitting the time-activity curve (TAC) from multiple SPECT/CT imaging timepoints.

### Challenge

- MTP imaging is resource-intensive, since the multiple SPECT scans increase burden on patients and clinical workflows.
- Established single time-point (STP) TIA estimation methods like Hänscheid (STP-H) [1] and Madsen (STP-M) [2] are proposed primarily for Lu-177 DOTATATE and may not fully capture the kinetics of Lu-177 PSMA dosimetry. Additionally, they rely on oversimplified assumptions of radiotracer decay fail to consider patient-specific parameters that might influence distribution patterns.

### Objective

- The objective of this study is to propose a graph neural network (GNN)-based STP TIA-estimation approach, which uses radiomic features extracted from a single SPECT/CT scan and predicts the TIA for eight organs-at-risk relevant to Lu-177 PSMA.
- This approach enables more personalized, efficient, and data-driven TIA estimation using a single imaging timepoint.
- Our proposed STP-GNN is evaluated against STP-H and STP-M using MTP-derived TIA as ground truth.

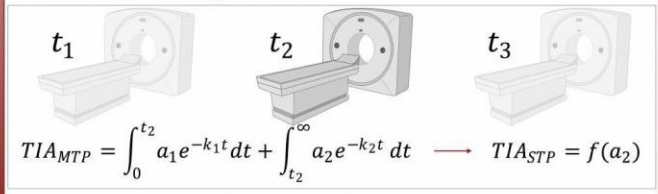


Fig. 1. Concept: STP as a practical alternative to MTP TIA estimation

## Methods

### Data Description and Processing

- We analyzed SPECT/CT scans from 34 patients undergoing Lu-177 PSMA therapy, encompassing 84 dose cycles with 2-3 imaging time-points acquired between 24- and 216-hours post-injection. SPECT images were registered to CT using SimpleITK on Python.
- Eight organs-at-risk (OARs) were selected for the TIA analysis, namely the spleen, right kidney, left kidney, gallbladder, liver, stomach, pancreas and the prostate. OAR segmentation was performed using the TotalSegmentator tool.
- 37 radiomic features were extracted for each OAR using PyRadiomics, including first-order intensity, shape, and texture-based features. Feature-wise normalization was performed to ensure stable learning.
- MTP dosimetry was performed by fitting the TAC with bi-exponential functions [3].
- Spatial proximity between each pair of OARs was derived from the CT scan as the edges, thus constructing and OAR-graph for each patient .
- The timepoint closest to 48 hours post-injection was chosen for all 3 methods as it was the optimal value for STP-M and STP-H.

### Network Architecture

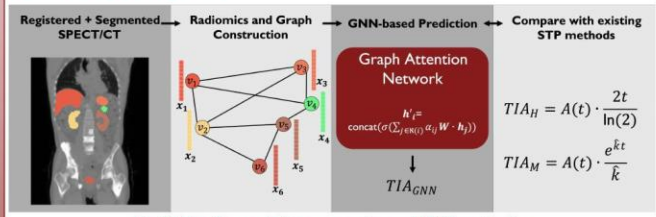


Fig. 2. Workflow of data processing and STP methods

- The train set encompassed 58 (70%) and the test set had 26 (30%) out of the 84 dose cycles across all subjects.
- The high-dimensional node inputs were passed through an encoder for feature reduction from 37 to 12.
- A graph attention network (GAT) was chosen as the GNN and implemented to predict OAR-specific TIA using z-score normalized radiomic features and inter-organ connectivity.
- The GAT model used 3 layers, 128 hidden channels, learning rate 5e-4, 500 epochs to predict the TIA (STP-GNN), compared with MTP TIA as ground truth using the L2 loss function.

## Results

- STP-GNN consistently outperformed both STP-H and STP-M across all metrics, demonstrating the lowest mean absolute error (MAE), root mean square error (RMSE) and normalized root mean square error (NRMSE) (0.2611, 0.5057, 0.2023), compared to STP-M (0.3252, 0.5866, 0.3083) and STP-H (0.4636, 0.9464, 0.3657).
- This trend is followed across individual OARs, with STP-GNN demonstrating the lowest variability across subjects.

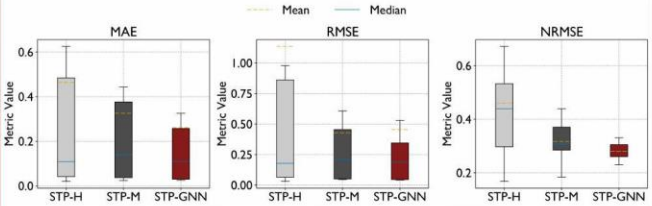


| OAR | STP-H | STP-M | STP-GNN |
|---|---|---|---|
| Spleen | 0.306 | 0.367 | 0.331 |
| Right Kidney | 0.487 | 0.302 | 0.264 |
| Left Kidney | 0.895 | 0.439 | 0.309 |
| Gall Bladder | 0.168 | 0.254 | 0.251 |
| Liver | 0.672 | 0.184 | 0.230 |
| Stomach | 0.272 | 0.314 | 0.269 |
| Pancreas | 0.464 | 0.382 | 0.305 |
| Prostate | 0.416 | 0.296 | 0.292 |

Fig. 3. (Top) Whisker plots of MAE, RMSE, and NRMSE across subjects (Bottom) OAR-wise NRMSE values for STP-H, STP-M, and STP-GNN

## Conclusions

- STP-GNN offers a fast, personalized alternative to empirical STP methods with superior accuracy and consistency.
- In future, we will extend our work to segmented lesions and investigate voxel-level STP methods.

## References

[1] Hänscheid H, Lapa C, Buck AK, Lassmann M, Werner RA. Dose Mapping After Endoradiotherapy with 177Lu-DOTATATE/DOTATOC by a Single Measurement After 4 Days. J Nucl Med. 2018;59:75-81.
[2] Madsen MT, Menda Y, O'Dorisio TM, O'Dorisio MS. Single time point dose estimate for exponential clearance. *Med Phys*. 2018;45:2318-2324.
[3] Ivashchenko OV, O'Doherty J, Hardiansyah D, et al. Time-Activity data fitting in molecular Radiotherapy: Methodology and pitfalls. *Phys Med*. 2024;117:103192.

# What is Wasserstein distance? A discrete case

Let us first look at a simple case where the probability domain is *discrete*. For example, suppose we have two distributions $P$ and $Q$, each has four piles of dirt and both have ten shovelfuls of dirt in total. The numbers of shovelfuls in each dirt pile are assigned as follows:

$$P_1 = 3, P_2 = 2, P_3 = 1, P_4 = 4$$
$$Q_1 = 1, Q_2 = 2, Q_3 = 4, Q_4 = 3$$

In order to change $P$ to look like $Q$, as illustrated in Fig. 7, we:

- First move 2 shovelfuls from $P_1$ to $P_2$ => $(P_1, Q_1)$ match up.
- Then move 2 shovelfuls from $P_2$ to $P_3$ => $(P_2, Q_2)$ match up.
- Finally move 1 shovelfuls from $Q_3$ to $Q_4$ => $(P_3, Q_3)$ and $(P_4, Q_4)$ match up.

If we label the cost to pay to make $P_i$ and $Q_i$ match as $\delta_i$, we would have $\delta_{i+1} = \delta_i + P_i - Q_i$

$$\delta_0 = 0$$
$$\delta_1 = 0 + 3 - 1 = 2$$
$$\delta_2 = 2 + 2 - 2 = 2$$
$$\delta_3 = 2 + 1 - 4 = -1$$
$$\delta_4 = -1 + 4 - 3 = 0$$

Finally the Earth Mover's distance is $W = \sum |\delta_i| = 5$.

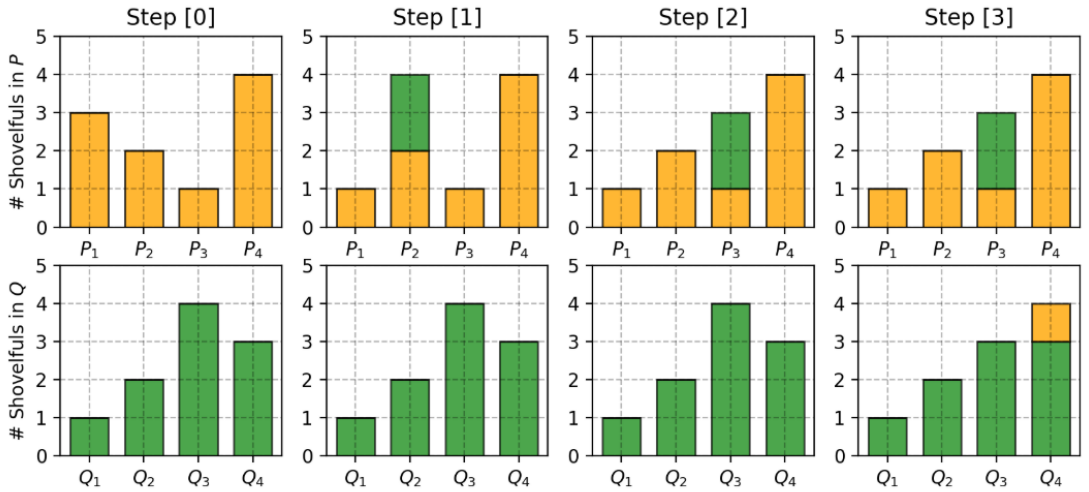


Figure 7: Step-by-step plan of moving dirt between piles in $P$ and $Q$ to make them match.